*Progress In Electromagnetics Research B, Vol. 14, 383–405, 2009*

# MORE EFFICIENCY OF TRANSVERSE WAVE APPROACH (TWA) BY APPLYING ANISOTROPIC MESH TECHNIQUE (AMT) FOR FULL-WAVE ANALYSIS OF MICROWAVE PLANAR STRUCTURES

**M. Ayari**

Department of mathematics
Virginia Polytechnic Institute and state university-Blacksburg
VA, USA

**T. Aguili**

Syscom Laboratory
National Engineering School
B.P 37 Le belvedere 1002 Tunis, Tunisia

**H. Baudrand**

EM Research & Design, RCEM
17 Rue Denis Papin, 31500 Toulouse, France

**Abstract**—The present paper sets out to present a numerical electromagnetic (EM) method TWA for EM field modeling of planar structures. Combining both the benefits of TWA process and the modeling of planar excitation source, an optimization technique AMT is applied and evaluated in context of RF integrated-circuit applications. The computational complexity of TWA process is examined and the obtained simulation results are found to be in good agreement with literature. Index Terms- Transverse wave approach (TWA), anisotropic mesh technique (AMT), computational complexity, planar structures

Corresponding author: M. Ayari (ayari@vt.edu).

## 1. INTRODUCTION

Since that time computer technology has grown at a staggering pace, the field of radio frequency (RF) and microwave design has followed closely behind. The extremely wide range of electromagnetic (EM) problems has made impossible to circumvent a rigorous EM analysis. This has urged the Scientifics' engineers and researchers to undertake many research efforts, during the last three decade, to develop a variety of new EM techniques, so-called numerical EM methods for EM field modeling because for many EM structures like antennas, active devices, microwave circuits and so forth, exact analytical solutions cannot be found. Overall, these methods are either differential or integral methods having their own benefits and limitations [1–13].

In order to obtain results with short CPU time, compactness memory and a good precision, these methods were readjusted for implementation of an original approach based on the transverse wave formulation [14].

Such a method, developed by our group and called-up Transverse Wave Approach (TWA), has several features that set it apart from other numerical EM methods.

Indeed, no matrix inversion is required by the TWA, no limitations on the shape of the components are imposed, no numerical instabilities often stemmed from the matrices with large condition number and the convergence are insured independently of the interfaces of analyzed structure. Besides, the TWA is based on transverse waves instead of the tangential EM fields that allow us to handle scattering operators rather than manipulating unbounded impedance or admittance operators [15, 16].

The nature of the excitation source implemented in TWA is one of the important characteristics of this approach. EM modeling of excitation source refers to the combined modeling between electromagnetic fields and linear and nonlinear circuits as mentioned in numerous scientific publications [17, 18].

For some numerical methods in electromagnetics such as the finite element method (FEM) [10–13, 19], finite-difference method (FDM) [2–4, 20–24], the transmission line matrix (TLM) [25–28] and method of lines (MoL) [29–32], the fundamental mode of transverse electric or transverse magnetic field of the studied structure is considered as an excitation source. This excitation mode is named extended source. In the integral methods as the method of moment (MoM) [6–9, 33], test functions are used as excitation source which can be defined either on the metal or on the dielectric sub-domains. This source will be electric or magnetic fields applied in the areas where the associated

wavelength g is less than the guided wavelength $\lambda_g$ is less than the guided wavelength $\lambda_s$ ($\lambda_s \ll \lambda_g$). The excitation mode is named localized source [34].

Identifying the excitation source is a difficult task [35] because the located active element at the time of simulation must faithfully satisfy the experimental conditions. In addition to the global description of the analyzed structure applied in an equivalent homogeneous milieu [36], the best solution is to adopt simple sources.

Therefore, the excitation source is defined by a function-level whose numerical implementation is simple compared to the localized or extended sources. In this paper, the advantages of the EM modeling of excitation source as mentioned earlier and the benefits of our numerical EM method TWA are gathered to open working space to apply an optimization technique called Anisotropic Mesh Technique (AMT), for a full-wave analysis of planar structures. The purpose is to obtain simulation results with a minimum of computational effort retaining sufficient accuracy.

Section 2 begins with theoretical background of TWA and presents a view of our approach. It also deals with EM modeling of both bilateral and unilateral excitation source and examines the convergence of TWA.

The computational complexity of TWA process is discussed in Section 3. In Section 4, a reference planar structure used in wireless communication systems is chosen for investigation and the obtained simulation results are in good agreement with literature, showing the efficiency of the TWA when the AMT technique is applied.

## 2. THEORY

Based on Hilbert Space methods, the wave concept is established to transform integral formulations of EM field to problems into algebraic ones. This concept is considered as one of the strong point of the TWA approach. It is built on the linear combination between transverse electric field $E_t$ and transverse magnetic field $H_t$ so as to obtain both incident $A_r$ and reflected $B_r$ waves from the discontinuity surface. These combinations can be expressed by:

$$\begin{vmatrix} A_r \\ B_r \end{vmatrix} = \hat{\boldsymbol{T}} \begin{vmatrix} E_t^r \\ H_t^r \times n_r \end{vmatrix} = \hat{\boldsymbol{T}} \begin{vmatrix} E_t^r \\ J_t^r \end{vmatrix} \tag{1}$$

where: $\hat{\boldsymbol{T}}$ ensures the transition between integral EM field and algebraic EM wave:

$$\hat{\boldsymbol{T}} = \frac{1}{2} \begin{vmatrix} Z_{0r}^{-1/2} & Z_{0r}^{1/2} \\ Z_{0r}^{-1/2} & -Z_{0r}^{1/2} \end{vmatrix} \tag{2}$$

and in return their connection is given by

$$\hat{\boldsymbol{T}}^{-1} = \begin{vmatrix} Z_{0r}^{1/2} & Z_{0r}^{1/2} \\ Z_{0r}^{-1/2} & -Z_{0r}^{-1/2} \end{vmatrix}. \tag{3}$$

where $Z_{0r} = \sqrt{\mu_0/\varepsilon_0\varepsilon_{r_r}}$ Real wave impedance from region $r \in \{1.2\}$ ($\mu_0$: Vacuum permeability; $\varepsilon_0$: Vacuum permittivity; $\varepsilon_{r_r}$: dielectric constant from region $r$); $n_r$: Outgoing normal vector oriented towards region $r$.

TWA presents many advantages in numerical EM techniques compared to other methods. In fact, no trial functions, no matrices inversions and no geometric constraint are imposed by our approach. The iterative process of TWA is based on the toggling between the spatial and modal wave expansions using mode-pixel transform. To insure this transformation in short computation time, we consider three different bases: Cartesian Basis (CB), Fourier Basis (FB) and Modal Basis (MB) where both incident $A_r$ and reflected $B_r$ waves are successively defined.

The transformation between CB and FB is ensured by Fast Fourier transform (FFT) and its inverse IFFT. FFT is nothing but an acceleration tool between spatial and modal domains.

The transformation of any vector from FB to MB is achieved by Fourier Modal Transform (FMT). These domains are related by their transition operator $\hat{\boldsymbol{P}}$ given by:

$$\hat{\boldsymbol{P}} = \begin{bmatrix} K_{mn}^{y} & -K_{mn}^{x} \\ K_{mn}^{x} & K_{mn}^{y} \end{bmatrix} \tag{4}$$

where

$$K_{mn}^{x} = \frac{m}{a} \cdot \left( \frac{m^2}{a^2} + \frac{n^2}{b^2} \right)^{-\frac{1}{2}}; \quad K_{mn}^{y} = \frac{n}{b} \cdot \left( \frac{m^2}{a^2} + \frac{n^2}{b^2} \right)^{-\frac{1}{2}} \tag{5}$$

$a$ and $b$ define the dimension of the metal box.

Or

$$\det(\hat{\boldsymbol{P}}) = K_{mn}^{y^2} + K_{mn}^{x^2} = 1 \tag{6}$$

The transformation from Fourier domain to Modal domain is accomplished by a rotation of angle $\theta$, given by:

$$\theta = \text{arctg}\,(K_{mn}^{x}/K_{mn}^{y}) \tag{7}$$

The inverse Fourier-Modal Transform (IFMT) can be obtained by its transition operator:

$$\hat{\boldsymbol{P}}^{-1} = \begin{bmatrix} K_{mn}^{y} & K_{mn}^{x} \\ -K_{mn}^{x} & K_{mn}^{y} \end{bmatrix} \tag{8}$$

Figure 1 illustrates the different transformations mentioned above.

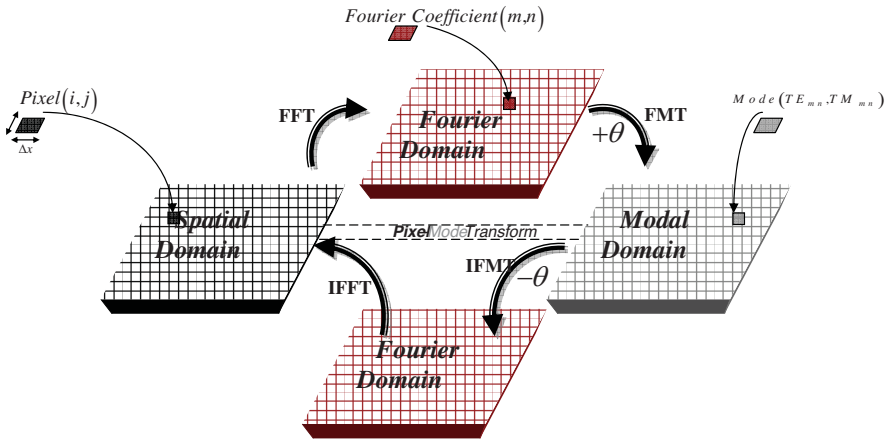


**Figure 1.** General principle of the Mode-Pixel and Pixel-Mode transforms.

The mutual coupling between incident ($A$) and reflected ($B$) waves leads to the scheme presented in the following:

$$\begin{cases} A = \hat{\boldsymbol{\Gamma}} B \\ B = \hat{\boldsymbol{S}} A + B^{(0)} \end{cases} \tag{9}$$

Where: $B^{(0)}$ is the global excitation wave on the source.

$\hat{S}$ is the spatial diffraction operator describing the boundary conditions from the discontinuity surface $\Omega$. This interface ($\Omega$) is divided into cells and can include four sub-domains: dielectric ($Di$), metal ($Me$), source ($Sce$) and surface impedance ($I_{surf}$).

Let $H_{\Omega_{SUB}}$ be an indicator function of the sub-domain $\Omega_{SUB}$ ($SUB$ refers to the nature of sub-domain: $Di, Me, Sce$ or $I_{surf}$) defined

by:

$$H_{\Omega_{SUB}}(u,v) = l_{\Omega_{SUB}}(u,v) = \begin{cases} 1 & \text{if } (u,v) \in \Omega_{SUB} \\ 0 & \text{Otherwise} \end{cases} \tag{10}$$

So, the air-dielectric interface $\Omega$ is characterized by the following relation:

$$H_{\Omega_{SUB=Sce}} + H_{\Omega_{SUB=Di}} + H_{\Omega_{SUB=Me}} + H_{\Omega_{SUB=I_{Surf}}} = 1 \tag{11}$$

Due to Eq. (9), the relationship between incident and reflected waves with $x$-component and y-component from each region $r = 1, 2$ can be written as:

$$\begin{aligned} \underbrace{\begin{bmatrix} B_1^x \\ B_1^y \\ B_2^x \\ B_2^y \end{bmatrix}}_{B} &= \hat{S} \underbrace{\begin{bmatrix} A_1^x \\ A_1^y \\ A_2^x \\ A_2^y \end{bmatrix}}_{A} + \underbrace{\begin{bmatrix} B_1^{(0)x} \\ B_1^{(0)y} \\ B_2^{(0)x} \\ B_2^{(0)y} \end{bmatrix}}_{B^{(0)}} \\ &= \overbrace{\begin{bmatrix} S^{x,11} & 0 & S^{x,12} & 0 \\ 0 & S^{y,11} & 0 & S^{y,12} \\ S^{x,21} & 0 & S^{x,22} & 0 \\ 0 & S^{y,21} & 0 & S^{y,22} \end{bmatrix}}^{\hat{s}} \begin{bmatrix} A_1^x \\ A_1^y \\ A_2^x \\ A_2^y \end{bmatrix} + \begin{bmatrix} B_1^{(0)x} \\ B_1^{(0)y} \\ B_2^{(0)x} \\ B_2^{(0)y} \end{bmatrix} \end{aligned} \tag{12}$$

The coefficients $(S^{c,r_1r_2})_{\substack{c=x,y \\ r_1,r_2\in\{1,2\}}}$ of $\hat{S}$ are given in Appendix A.

Also, on the $\Omega_{SUB}$ sub-domain, the waves A and B are connected by $\boldsymbol{S}_{\Omega_{SUB}}$ as follows:

$$\underbrace{\begin{bmatrix} B_1^x \\ B_1^y \\ B_2^x \\ B_2^y \end{bmatrix}}_{B} = \boldsymbol{S}_{\Omega_{SUB}} \underbrace{\begin{bmatrix} A_1^x \\ A_1^y \\ A_2^x \\ A_2^y \end{bmatrix}}_{A} \tag{13}$$

As a result, $\hat{\boldsymbol{S}}$ can be taken under the following form:

$$\hat{\boldsymbol{S}} = \Sigma_{SUB} \boldsymbol{S}_{\Omega_{SUB}} \hat{\boldsymbol{H}}_{\Omega_{SUB}} \tag{14}$$

where $\hat{\boldsymbol{H}}_{\Omega_{SUB}}$ is the projection operator given in Dirac notation:

$$\hat{\boldsymbol{H}}_{\Omega_{SUB}} = \left|H_{\Omega_{SUB}}(u,v)\right\rangle\left\langle H_{\Omega_{SUB}}(u,v)\right| \tag{15}$$

In Dirac notation, the reflection operator $\hat{\Gamma}$ can be written as:

$$\hat{\boldsymbol{\Gamma}} = \sum_{\alpha=TE,TM}\sum_{m}^{M_x}\sum_{n}^{M_y}\left|f^{\alpha}_{mn}\right\rangle\Gamma^{\alpha}_{mn}\left\langle f^{\alpha}_{mn}\right| \tag{16}$$

where: $\Gamma^{\alpha}_{mn}$ are the modal reflection coefficients or the eigenvalues of $\hat{\Gamma}$ whose expression for each mode $\alpha = TE, TM$ and each region $r$. These expressions are given in Appendix B.

$\{|f^{\alpha}_{mn}\rangle\}$ are Transverse TE and TM Eigenfunctions of $\hat{\Gamma}$ verifying $\langle f^{\alpha}_{p,q}|f^{\alpha}_{p',q'}\rangle = \delta^{p,p'}_{q,q'}$†. Their expressions are also given in Appendix B.

### 2.1. EM Modeling of Excitation Source

On the surface $\Omega_{SUB=Sce}$, a magnetic excitation source (MES) or an electric excitation source (EES) can be disposed to ensure the mutual coupling between tangential electric fields respectively, and tangential magnetic fields on both sides of this surface as it expresses the imposition of a jump value on the surface of the electric respectively magnetic field [37, 38]. They are represented by ideal generators as depicted in Figure 2.

The circuit which is connected to the source fixed the dual quantity of the source on its sub-domain $\Omega_{SUB=Sce}$. The surfacic wave sources (SWS) excite equally both sides of the surface; hence, we talk about bilateral source. It is for this reason that we introduce in the scheme of Figure 3 as a quadrupole [39]. Furthermore, it is not possible to impose simultaneously on a single surface a jump of both electric and magnetic field. In terms of circuit, a SWS does not fix the quantity $A + B$ or $A - B$, it solely determines $A$ or $B$ as the conventions were adopted.

The transfer of electromagnetic fields into circuit current and voltage parameters depends on the dimension of SWS ($l_s \times w_s$), taking the following form:

$$\begin{bmatrix} V \\ I \end{bmatrix} = \begin{bmatrix} l_s & 0 \\ 0 & w_s \end{bmatrix}\begin{bmatrix} \hat{E} \\ \hat{J} \end{bmatrix} \tag{17}$$

† $\delta^{p,p'}_{q,q'}$ denotes the kronecker symbol. It is equal to 1 if $(p,q) = (p',q')$ and 0 otherwise.

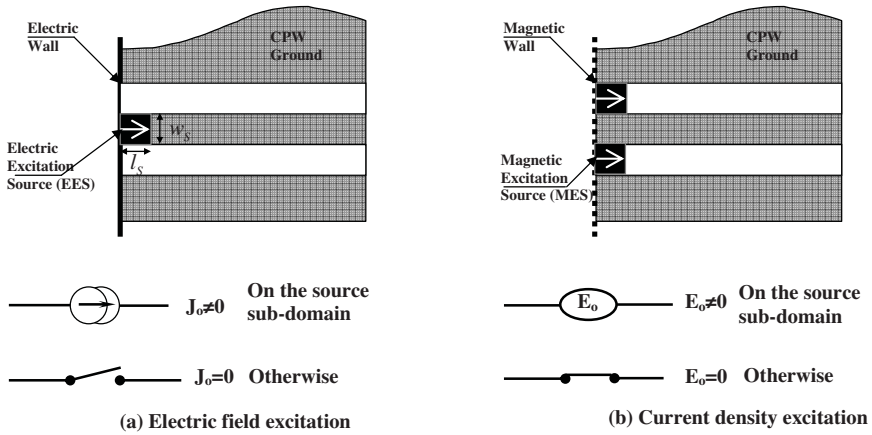


**Figure 2.** Representation of both electric field and current density excitation.

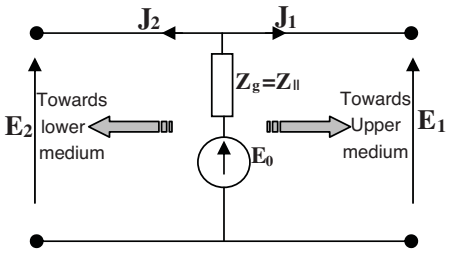


**Figure 3.** Equivalent circuit of bilateral planar excitation source.

where $\hat{E}$ and $\hat{J}$ are respectively the tangential electric and magnetic fields on source sub-domain $\Omega_{SUB=S}$ given by:

$$\begin{cases} \hat{E} = \sum\limits_{\Omega_{SUB=Sce}} E_T \\ \hat{J} = \sum\limits_{\Omega_{SUB=Sce}} \left( J_1^{r=1} + J_2^{r=2} \right) \end{cases} \tag{18}$$

Indeed, the SWS is characterized by the coefficient of reflection that feeds the circuit; in turn, the circuit fed by SWS is characterized by the coefficient of reflection that it presents on this source. Its input impedance is thus determined by comparison with the generator internal impedance, which is arbitrary chosen. Thus, SWS includes internal impedance $Z_g$.

Returning to the bilateral SWS, the quadrupole depicted in

Figure 3 is constituted by ideal voltage generator $E_0$ in series with the internal impedance $Z_g$. We assume that $Z_g$ be parallel impedance between two regions. It can be expressed by:

$$Z_g = Z_{\parallel} = Z_{01}Z_{02}/(Z_{01} + Z_{02}) \tag{19}$$

Based on the electric equivalent circuit shown above and using Ohm's law, the equation relating electric field with current density on both mediums can be written as:

$$E_1 = E_2 = E_0 - Z_{\parallel} \times (J_1 + J_2) \tag{20}$$

Assuming that the bilateral excitation source is polarized in $x$-direction and referring to equations Eq. (12) up to Eq. (15) and Eq. (20), the connection matrix between incident and reflected waves leads to:

$$S_{\Omega_{SUB=Sce}} = \begin{bmatrix} 1/2(-1+\rho_1+\rho_1) & 0 & (\rho_1 \times \rho_2)^{1/2} & 0 \\ 0 & -1 & 0 & 0 \\ (\rho_1 \times \rho_2)^{1/2} & 0 & 1/2(-1-\rho_1+\rho_2) & 0 \\ 0 & 0 & 0 & -1 \end{bmatrix} \tag{21}$$

where

$$\rho_r = Z_{\parallel}/Z_{0r}; \quad r = 1, 2 \tag{22}$$

Also, from (9) the global excitation wave $B^{(0)}$ on the interface is connected to the EM excitation field $E_0$ by:

$$\begin{bmatrix} B_1^{(0)x} \\ B_1^{(0)y} \\ B_2^{(0)x} \\ B_2^{(0)y} \end{bmatrix} = \begin{bmatrix} Z_{01}^{-1/2}/2 \\ 0 \\ Z_{02}^{-1/2}/2 \\ 0 \end{bmatrix} E_0 \tag{23}$$

Suppose at a moment that the source can be reduced to a dipole instead of quadrupole. It must hence be assumed that only a half-space is lighted and that the surface is based on a wave screen; hence, we talk about unilateral excitation source.

Indeed, the unilateral SWS generate waves in one of two dielectric environments from discontinuity interface $\Omega$. The quadruple depicted in Figure 4 treats the case where the excitation source SWS is oriented towards upper medium (region 2).

In this scenario, the SWS introduces an incident wave in this region while in the lower medium (region1) the source behaves like pure metal, hence the non excited area is modeled by an interrupting

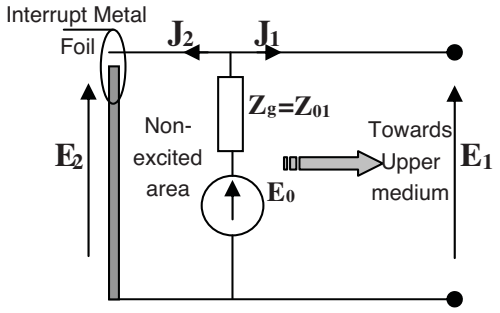


**Figure 4.** Equivalent circuit of unilateral planar excitation source in upper medium.

thin metal foil since the screen effect resulting from a local weakening of external magnetic field due to the presence of SWS [40] interrupted the continuity of EM fields crossing the dielectric interface on the source sub-domain $\Omega_{SUB=Sce}$.

Based on Ohm's law, we can deduce from electric equivalent circuit shown in Figure 4 the relation between electric field and current density on both:

In upper medium

$$E_1 = E_0 - Z_{\|} \times (J_1 + J_2) \tag{24}$$

In lower medium

$$E_2 = 0 \tag{25}$$

Using the polarization in $x$-direction, the sub-domain source $\Omega_{SUB=Sce}$ on $y$-direction will behave like metal domain. Therefore the general expression of $\boldsymbol{S}_{\Omega_{SUB=Sce}}$ can be expressed as:

$$\boldsymbol{S}_{\Omega_{SUB=Sce}} = \begin{bmatrix} 1-u & 0 & \rho(2-u) & 0 \\ 0 & -1 & 0 & 0 \\ \rho^{-1}(u-1) & 0 & u-2 & 0 \\ 0 & 0 & 0 & -1 \end{bmatrix} \tag{26}$$

where $\rho = \sqrt{Z_{01}/Z_{02}}$.

And the excitation wave $B^{(0)}$ can be written in this case as:

$$\begin{bmatrix} B_1^{(0)x} \\ B_1^{(0)y} \\ B_2^{(0)x} \\ B_2^{(0)y} \end{bmatrix} = \begin{bmatrix} (u-1)Z_{01}^{-1/2}/2 \\ 0 \\ (2-u)Z_{02}^{-1/2}/2 \\ 0 \end{bmatrix} E_0 \tag{27}$$

With: $u = 1$; Unilateral excitation source towards upper medium (region1)

$u = 2$; Unilateral excitation source towards lower medium (region2)

The polarization in $y$-direction can be found in appendix.

The benefits which the TWA can attain due to the selection of the polarization direction will be appeared in Section 4.

### 2.2. Convergence of TWA

The system depicted in Eq. (9) leads to an iterative scheme by starting from the wave excitation source as shown below:

$$\begin{cases} B^{(0)} = B^{(0)} \\ A^{(n)} = \hat{\mathbf{\Gamma}} B^{(n-1)} \\ B^{(n)} = \hat{\boldsymbol{S}} A^{(n)} + B^{(0)} \end{cases} \tag{28}$$

where $(n)$ denotes the iteration order.

$\hat{\mathbf{\Gamma}}$ and $\hat{\boldsymbol{S}}$ are two linear operators in Hilbert space. Therefore the system (28) can be rewritten as:

$$\begin{cases} B^{(0)} = B^{(0)} \\ A^{(n)} - A^{(n-1)} = \hat{\mathbf{\Gamma}} \left( B^{(n-1)} - B^{(n-2)} \right) \\ B^{(n)} - B^{(n-1)} = \hat{\boldsymbol{S}} \left( A^{(n)} - A^{(n-1)} \right) \end{cases} \tag{29}$$

Let $\Delta W^{(n)}$ be the difference, in term of waves, between two successive waves $W^{(n)}$ and $W^{(n-1)}$ at, respectively, iteration $(n)$ and iteration $(n-1)$ where $W$ refers to $A$ or $B$. This can be expressed as follows:

$$\begin{cases} A^{(n)} = \Delta A^{(n)} + \Delta A^{(n-1)} + \cdots + \Delta A^{(2)} + \hat{\mathbf{\Gamma}} B^{(0)} \\ B^{(n)} = \Delta B^{(n)} + \Delta A^{(n-1)} + \cdots + \Delta B^{(1)} + B^{(0)} \end{cases} \tag{30}$$

From (29) and terms of (31), we obtain

$$\begin{cases} \Delta B^{(n)} = (\hat{S}\hat{\Gamma})^n B^{(0)} \\ \Delta A^{(n)} = (\hat{\Gamma}\hat{S})^{n-1} \hat{\Gamma} B^{(0)} \end{cases} \tag{31}$$

The convergence of (29) is reached when the norms $\|\Delta B^{(n)}\| \to 0$ and $\|\Delta A^{(n)}\| \to 0$. The convergence speed is driven by the sectral radius of $\|\hat{S}\hat{\Gamma}\|$ and $\|\hat{\Gamma}\hat{S}\|$.

The unitarity of the reflection operator $\hat{\Gamma}$ [41, 42] and the spectral radius of $\hat{S}$ that it is less than unity when the losses are taken into account proves that the spectral radius of $\|\hat{S}\hat{\Gamma}\|$ and $\|\hat{\Gamma}\hat{S}\|$ are less than 1; hence the convergence of TWA is well verified.

Furthermore, the observation of the convergence can be established by the computation of input impedance $\boldsymbol{Z}_{in}$ on the source sub-domain $S_{\Omega_{SUB=Sce}}$:

$$Z_{in}^{(k)} = \frac{\sum\limits_{\Omega_{SUB=Sce}} E^{(k)}}{\sum\limits_{\Omega_{SUB=Sce}} \left(J_1^{(k)} + J_2^{(k)}\right)^*} \times \left(\frac{l_s}{w_s}\right)^{\tau} \tag{32}$$

where

$J_1^{(n)}$: Current density in each region $i$ at iteration $(n)$.

$E^{(n)}$: Electric field in excitation side at iteration $(n)$.

The term $(\frac{l_s}{w_s})^{\tau}$ is often so-called the form factor of excitation source; $l_s$ and $w_s$ are respectively the length and width of the source.

$\tau$ depends on the source polarization; $\tau = 1$ polarization in $x$-direction and $\tau = -1$ polarization in $y$-direction.

## 3. COMPLEXITY OF THE TWA ALGORITHM

In order to prove the efficiency of our EM method, it is important to measure the quality of its algorithm especially the computational complexity at the time of the implementation of the TWA algorithm.

Indeed, let $N_T = M_x \times N_y$ be the total number of pixels required for TWA process for single metal interface and $N_{iter}$ be the iteration number the convergence of TWA method needs (generally about 100); assuming that total number of modes is equal to total number of pixels, the complexity of TWA algorithm with the asymptotic notation is $O(N_{iter} N_T^2 \log N_T)$.

Supposing $N_{TWA}$ the CPU number operations of TWA and comparing it with the one of other EM numerical methods like conventional Method of Moment (MoM) [12–40] (without any fast procedure) let $N_{MOM}$, we obtain therefore these results:

$N_{TWA}/N_{MOM} \prec 1$ for low complexity problems ($N_T \prec 2^{12}$) and

$N_{TWA}/N_{MOM} \prec 10^{-6}$ for high complexity problems ($N_T \gg 2^{12}$)

This $N_{TWA}$ can be reduced without applying any speeding algorithm at an important rate when we use an optimization technique related to TWA which is the main subject of the next section.

**Table 1.** Comparison between TWA and MoM into number of operations.

| | |
|---|---|
| For low complexity problems ($N_T \prec 2^{12}$) | $N_{TWA}/N_{MoM} \prec 1$ |
| For high complexity problems ($N_T \succ 2^{12}$) | $N_{TWA}/N_{MoM} \prec 10^{-6}$ |

## 4. SIMULATION RESULTS

During recent decades wireless communication systems have been developed to satisfy continually increasing demands for personal, local, mobile and satellite communications by enhancing and replacing wire-media loops with wireless communication media [43].

The optimal frequency band for each propagation channel is determined and limited by the technical requirements of each communication system and by the conditions of radio propagation through each channel. Moreover, radio waves with frequencies higher than 3 GHz (C, X, K bands, up to several hundred GHz, which are also loosely described as microwaves) have begun to be used for constructing new kinds of wireless communication channels whose characteristics are studied in many scientific publications [44–46].

A wide range of planar printed antennas for wireless communication has been carefully presented and investigated in [47–49].

In this section we propose to simulate, as planar structure belonging to wireless communication systems, a 30 GHz microstrip patch antenna.

In order to enhance the performance and the efficiency of our EM method, an optimization technique will be applied to this structure. Excellent agreement will be observed between our obtained simulation results (with and without optimization) and literature.

### 4.1. Microstrip Patch Antenna

The application that was run of the TWA code was that of a microstrip patch antenna as depicted in Figure 5.

The choice of this application offers the possibility to define, in the context of circuit simulations, a planar source SWS exciting this antenna that we proposed bilateral polarized in $x$-direction.

To avoid the interaction of the antenna with boundary (problems

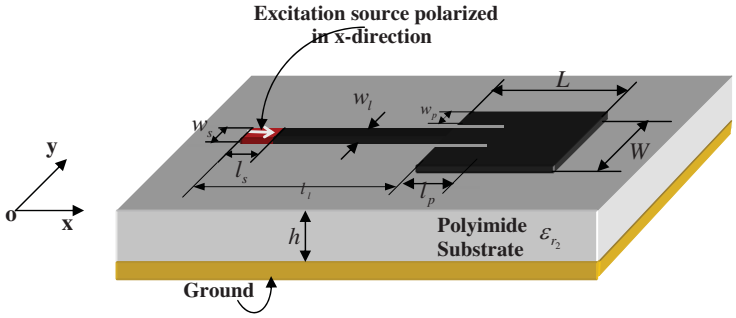


**Figure 5.** Microstrip fed patch antenna.

posed by the existence of periodic walls) [50, 51], the antenna was placed in the middle on discontinuity surface; an important space from boundary is considered as shown in Table 2.

Further, the test structure is based on a design for a 30 GHz patch antenna built on a thin polyimide film [52].

### 4.2. Anisotropic Mesh Technique (AMT)

In most EM applications, the applied meshing to the studied microwave structure was uniform and isotropic on both $x$ and $y$-direction [15, 16, 50] because of the nature of the existing excitation source as already mentioned in Section 2.

Our approach offers the possibility to tackle this problem by the presence of SWS. Indeed, keeping the details of circuit, an anisotropic mesh can be applied for this microwave structure polarized in L-direction ($L$ refer to $x$ or $y$) while considering only a refined meshing in polarization-direction i.e., this mesh follows the $L$-ward propagating signal generated by SWS.

In what follows, we shall simulate the 30 GHz patch antenna with and without this optimization technique AMT while comparing to reference [52].

Table 1 exhibits the different geometric and modeling simulation parameters for EM investigation of this antenna presented in Figure 5.

On one hand, the comparison between the simulated results (without AMT) obtained by our EM simulation software based on TWA method [53] for the reference structure and those obtained in [52] shows a satisfactory agreement.

On the other hand, once the previous result $S11$ plot is validated for this antenna we compare it with the $S11$ plot obtained by AMT technique where the meshing resolution is equal to $16\times256$; an excellent

**Table 2.** Geometric and modeling simulation parameters.

| | | Without AMT | With AMT |
|---|---|---|---|
| **Geometric Simulation Parameters** | Meshing Resolution | $256\times256$ | $16\times256$ |
| | Dimension of metal box | $a=10.496mm$ | |
| | | $b=10.496mm$ | |
| | Width of patch | $W=3239\mu m=79cells$ | |
| | Length of patch | $L=2624\mu m=64cells$ | $L=2624\mu m=4cells$ |
| | Length of microstrip line | $l_l=3936\mu m=96cells$ | $l_l=3936\mu m=6cells$ |
| | Width of microstrip line | $w_l=451\mu m=11cells$ | |
| | Length $l_p$ | $l_p=656\mu m=16cells$ | $l_p=656\mu m=1cell$ |
| | With $w_p$ | $w_p=1148\mu m=28cells$ | |
| | Dimension of source | $l_s=11cells$ | |
| | | $w_s=16cells$ | $w_s=1cell$ |
| | Form factor of source | $l_s/w_s=0.6875$ | |
| | Height of substrate | $h=511.3\mu m$ | |
| **Modeling Simulation Parameters** | Nature of metal box | Periodic walls | |
| | Type of polarization | $\tau=-1$ (bilateral in x-direction) | |
| | Number of iteration | $N_{iter}=300$ | |
| | Value of surface impedance | $Z_s=0$ | |
| | Permittivity of regions | $\varepsilon_{r_1}=1$ | |
| | | $\varepsilon_{r_2}=3.2$ | |
| | Waveband | $F_{\min}=28GHz$ | |
| | | $F_{\max}=35GHz$ | |
| | | $Step\_F_{rq}=0.1GHz$ | |

agreement has been observed between these simulations as shown in Figure 6.

The passing from a refined meshing to a coarser representation with the AMT technique leads to a certain accuracy of the simulation results. It can be seen from the $S11$ plot that there is a very small difference between the simulations (approx 1.5%) in the resonance frequency of the antenna.

This technique, as long as its effects on the electromagnetic behavior of the circuit remain negligible, results in significant reduction of the computation complexity.

There is no doubt that the type of processor and total memory installed on each node, and the speed and topology of the network connections are one of the important factors for an efficient

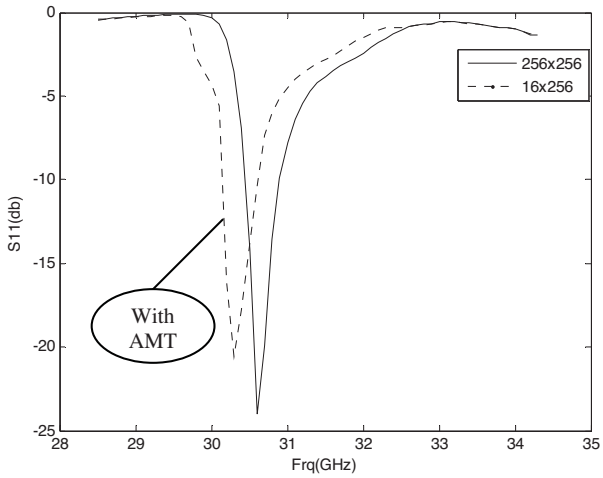


**Figure 6.** $S11$ of patch antenna with/without AMT.

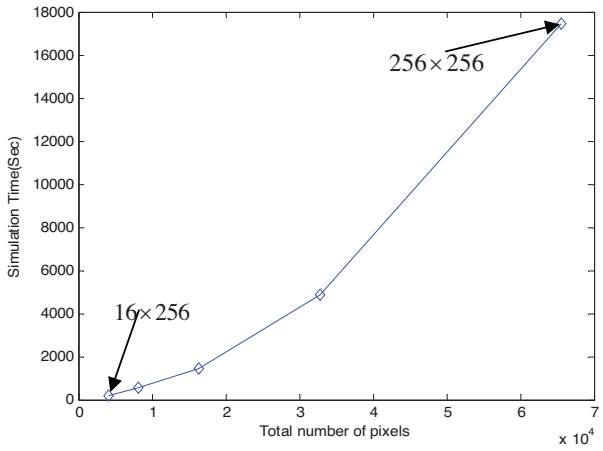


**Figure 7.** CPU time consumed to simulate the analyzed structure as function of meshing resolution.

implementation of EM method, leading to rapid EM simulation. However, in our case the TWA code are executed on a Pentium M processor 1.6 GHz with a RAM of 1 GHz and without any fast algorithm.

Figure 7 exhibits the CPU time consumed to simulate the studied structure for different resolutions (total number of meshing cells: $N_T$) and shows that for $N_T = 16 \times 256$ (i.e., with AMT) is about 85 times

faster, in terms of CPU, than in the case when $N_T = 256 \times 256$ (i.e., without AMT). In this case, the term $N_T^2 = M_x^2 \times N_y^2$ in the computational complexity of TWA process can be reduced to $M_x \times N_y^2$ which proves the usefulness of the AMT technique in TWA mainly in the high complexity problem.

## 5. CONCLUSION

In this paper, the numerical EM method TWA combined with the modeling of the excitation source SWS has been presented and successfully implemented for full-wave analysis of planar structures. The AMT technique has been applied to a 30 GHz patch antenna and the significant reduction in CPU time computation has demonstrated their efficiency to an improved version of TWA process in the context of RF integrated-circuit applications.

However, in RFIC where applications needed very high meshing resolution, the TWA becomes slower even if AMT is applied. Therefore, merging the benefits of Non-Uniform Fast Fourier Transform (NUFFT) and AMT technique in TWA process can be a good solution to tackle this problem.

## APPENDIX A. OPERATOR $\hat{S}$

The diffraction coefficients of operator $\hat{S}$ are computed for any excitation source (bilateral, unilateral towards region1 or region2) polarized either in $x$-direction or $y$-direction from pixel $(i, j)$:

$$\begin{aligned}
S_{ij}^{c,11} &= -\kappa_1 H_{\Omega_{SUB=Di}}(i,j) - H_{\Omega_{SUB=Me}}(i,j) + \xi_{11}^c H_{\Omega_{SUB=Sce}}(i,j) \\
&\quad + \upsilon_{11} H_{\Omega_{SUB=Isurf}}(i,j) \\
S_{ij}^{c,12} &= \kappa_2 H_{\Omega_{SUB=Di}}(i,j) + \xi_{12}^c H_{\Omega_{SUB=Sce}}(i,j) + \upsilon_{12} H_{\Omega_{SUB=Isurf}}(i,j) \\
S_{ij}^{c,21} &= \kappa_2 H_{\Omega_{SUB=Di}}(i,j) + \xi_{21}^c H_{\Omega_{SUB=Sce}}(i,j) + \upsilon_{21} H_{\Omega_{SUB=Isurf}}(i,j) \\
S_{ij}^{c,22} &= \kappa_1 H_{\Omega_{SUB=Di}}(i,j) - H_{\Omega_{SUB=Me}}(i,j) + \xi_{22}^c H_{\Omega_{SUB=Sce}}(i,j) \\
&\quad + \upsilon_{22} H_{\Omega_{SUB=Isurf}}(i,j)
\end{aligned}$$

where:

$$\begin{aligned}
\kappa_1 &= (\rho^2 - 1)\left(\rho^2 + 1\right)^{-1} \\
\kappa_2 &= 2\rho\left(\rho^2 + 1\right)^{-1} \\
\upsilon_{11} &= \left(Z_s(1 - \rho^2) + Z_{01}\right)\left(Z_s\left(1 + \rho^2\right) + Z_{01}\right)^{-1}
\end{aligned}$$

$$\upsilon_{12} = \upsilon_{21} = 2\rho Z_s \left(Z_s(1+\rho^2) + Z_{01}\right)^{-1}$$
$$\upsilon_{22} = \left(Z_s(\rho^2-1) + Z_{01}\right)\left(Z_s\left(\rho^2+1\right) + Z_{01}\right)^{-1}$$

For a bilateral excitation source:

$$\xi_{11}^x = \frac{(1+\tau)}{4}(-1+\rho_1-\rho_2) + \frac{(\tau-1)}{2}$$
$$\xi_{11}^y = \frac{(1-\tau)}{4}(-1+\rho_1-\rho_2) - \frac{(1+\tau)}{2}$$
$$\xi_{21}^x = \xi_{12}^x = \frac{(1+\tau)}{2}\sqrt{\rho_1\rho_2}$$
$$\xi_{21}^y = \xi_{12}^x = \frac{(1-\tau)}{2}\sqrt{\rho_1\rho_2}$$
$$\xi_{22}^x = \frac{(1+\tau)}{4}(-1-\rho_1+\rho_2) + \frac{(\tau-1)}{2}$$
$$\xi_{22}^y = \frac{(1-\tau)}{4}(-1-\rho_1+\rho_2) - \frac{(1+\tau)}{2}$$

For a unilateral excitation source:

$u = 1$; Unilateral excitation source towards upper medium (region1)

$u = 2$; Unilateral excitation source towards lower medium (region2)

$$\xi_{11}^x = \frac{(1+\tau)}{2}(1-u) + \frac{(\tau-1)}{2}$$
$$\xi_{11}^y = \frac{(1-\tau)}{2}(1-u) - \frac{(1+\tau)}{2}$$
$$\xi_{12}^x = (1+\tau)\rho(2-u)$$
$$\xi_{12}^y = \frac{(1-\tau)}{2}\rho(2-u)$$
$$\xi_{21}^x = (1+\tau)\rho^{-1}(u-1)$$
$$\xi_{21}^y = \frac{(1-\tau)}{2}\rho^{-1}(u-1)$$
$$\xi_{22}^x = \frac{(1+\tau)}{2}(u-2) + \frac{(\tau-1)}{2}$$
$$\xi_{22}^y = \frac{(1-\tau)}{2}(u-2) - \frac{(1+\tau)}{2}$$

where:

Polarization in $x$-direction: $\tau = 1$

Polarization in $y$-direction: $\tau = -1$

$Z_s$ : Complex surface impedance; $Z_{01}$: real wave impedance defined in Eq. (3)

$\rho = \sqrt{Z_{01}/Z_{02}}$; $\rho_r = Z_{\|}/Z_{0r}$; $r = 1, 2$ where $Z_{\|}$ is defined in Eq. (19).

## APPENDIX B. OPERATOR $\hat{\Gamma}$

1- TE and TM Eigenfuctions of reflection operator $\hat{\Gamma}$

| Mode TE | Mode TM |
|---|---|
| $\begin{cases} \vec{f}^{TE}_{mnx} = (ab)^{-\frac{1}{2}} K^{y}_{mn} e^{-j\frac{2m\pi}{a}x} e^{-j\frac{2n\pi}{b}y} \\ \vec{f}^{TE}_{mny} = -(ab)^{-\frac{1}{2}} K^{x}_{mn} e^{-j\frac{2m\pi}{a}x} e^{-j\frac{2n\pi}{b}y} \end{cases}$ | $\begin{cases} \vec{f}^{TM}_{mnx} = (ab)^{-\frac{1}{2}} K^{x}_{mn} e^{-j\frac{2m\pi}{a}x} e^{-j\frac{2n\pi}{b}y} \\ \vec{f}^{TM}_{mny} = (ab)^{-\frac{1}{2}} K^{y}_{mn} e^{-j\frac{2m\pi}{a}x} e^{-j\frac{2n\pi}{b}y} \end{cases}$ |

$K^{x}_{mn}, K^{y}_{mn}$ are defined in Eq. (5)

2- TE and TM Eigenvalues of $\hat{\Gamma}$:

| | | |
|---|---|---|
| **Mode TE** | Region 1 | $\Gamma^{TE,1}_{mn} = \left(1 + j\gamma_{mn,1}k_0^{-1}\varepsilon_{r_1}^{-1/2}\right)\left(1 - j\gamma_{mn,1}k_0^{-1}\varepsilon_{r_1}^{-1/2}\right)^{-1}$ |
| | Region 2 | $\Gamma^{TE,2}_{mn} = \left(1 + j\gamma_{mn,2}k_0^{-1}\varepsilon_{r_1}^{-1/2}\coth\left(\gamma_{mn,2}H\right)\right)\left(1 - j\gamma_{mn,2}k_0^{-1}\varepsilon_{r_1}^{-1/2}\coth\left(\gamma_{mn,2}H\right)\right)^{-1}$ |
| **Mode TM** | Region 1 | $\Gamma^{TM,1}_{mn} = \left(1 - jk_0\gamma^{-1}_{mn,1}\varepsilon_{r_1}^{-1/2}\right)\left(1 + jk_0\gamma^{-1}_{mn,1}\varepsilon_{r_1}^{-1/2}\right)^{-1}$ |
| | Region 2 | $\Gamma^{TM,2}_{mn} = \left(1 - jk_0\gamma^{-1}_{mn,2}\varepsilon_{r_2}^{-1/2}\coth\left(\gamma_{mn,2}H\right)\right)\left(1 + jk_0\gamma^{-1}_{mn,2}\varepsilon_{r_2}^{-1/2}\coth\left(\gamma_{mn,2}H\right)\right)^{-1}$ |

$\gamma_{mn,i} = \left(\left(\frac{m\pi}{a}\right)^2 + \left(\frac{n\pi}{b}\right)^2 - k_0^2\varepsilon_{r_i}\right)^{1/2}$: Propagation constant from region $i$.

$k_0 = \omega/c$: Angular EM wavenumber; $\omega$ angular frequency of the wave and $c$ speed of light in the vacuum of free space.

## REFERENCES

1. Liu, X., B.-Z.Wang, and S. Lai, "Element-free Galerkin method in electromagnetic scattering field computation," *Journal of Electromagnetic Waves and Applications*, Vol. 21, No. 14, 1915–1923, 2007.
2. Warnick, K. F., "An intuitive error analysis for FDTD and

comparison to MoM," *IEEE Antenna and Propagation Magazine*, Vol. 47, 111–115, Dec. 2005.

3. Kung, F. and H. T. Chuah, "Stability of classical finite-difference time-domain (FDTD) formulation with nonlinear elements — A new perspective," *Progress In Electromagnetics Research*, PIER 42, 49–89, 2003
4. Booton, R. C., *Computational Methods for Electromagnetics and Microwaves*, John Wiley & Sons, New York, 1992.
5. Yamashita, E., *Analysis method for EM Wave Problems*, Artech House, Boston, London, 1990.
6. Warnick, K. F. and W. C. Chew, "Error analysis of MoM," *IEEE Antenna and Propagation Magazine*, Vol. 46, 38–53, Dec. 2004.
7. Hatamzadeh-Varmazyar, S., M. Naser-Moghadasi, and Z. Masouri, "A moment method simulation of electromagnetic scattering from conducting bodies," *Progress In Electromagnetics Research*, PIER 81, 99–119, 2008.
8. Wang, J. J., *Generalized MoM in Electromagnetics*, John Wiley & Sons, New York, 1991.
9. Papakanellos, P. J., "Accuracy and complexity assessment of subdomain moment methods for arrays of thin-wire loops," *Progress In Electromagnetics Research*, PIER 78, 1–15, 2008.
10. Ozgun, O. and M. Kuzuoglu, "Finite element analysis of electromagnetic scattering problems via iterative leap-field domain composition method," *Journal of Electromagnetic Waves and Applications*, Vol. 22, 251–266, 2008.
11. Bedrosian, G., "High-performance computing for finite element methods in low-frequency electromagnetics," *Progress In Electromagnetics Research*, PIER 07, 57–110, 1993.
12. Itoh, T., *Numerical techniques for Microwave and Millimeter-Wave Passive Structures*, John Wiley & Sons, New York, 1989.
13. Davidson, D. B., *Computational Electromagnetics*, Cambridge University Press, Cambridge, 2005.
14. Ayari, M., T. Aguili, H. Temimi, and H. Baudrand, "An extended version of Transverse Wave Approach (TWA) for full-wave investigation of planar structures," *Journal of Microwave, Optoelectronics and Electromagnetic Applications*, Vol. 7, No. 2, Dec. 2008.
15. Wane, S., D. Bajon, and H. Baudrand, "Full-wave analysis of inhomogeneous deep-trench isolation patterning for substrate coupling reduction and Q-factor improvement," *IEEE Transactions on Microwave Theory and Techniques*, Vol. 54, No. 12, Dec. 2006.

16. Wane, S., D. Bajon, and H. Baudrand, "A new full-wave hybrid differential-integral approach for the investigation of multilayer structures," *IEEE Transactions on Microwave Theory and Techniques*, Vol. 53, No. 1, Jan. 2005.
17. Taillardat, Ph., H. Aubert, and H. Baudrand, "A combination of quasi-static approach with an integral method for the characterisation of microwave planar circuits," *IEEE Symp. MTT-S*, Vol. 1, 17-420, San Diego, May 1994.
18. Horng, T. S., W. E. McKinzie, and N. G. Alexopoulos, "Full-wave spectral domain analysis of compensation of microstrip discontinuities using triangular sub-domain functions," *IEEE Trans. MTT*, Vol. MTT-40, No. 12, 2137–2148, Dec. 1992.
19. Khan, R. L. and G. I. Costache, "Finite element method applied to modeling crosstalk problems on printed circuits boards," *IEEE Trans. Elect. Comp.*, Vol. 31, 5–15, Feb. 1989.
20. Gong, Z. and G.-Q. Zhu, "FDTD analysis of an anisotropically coated missile," *Progress In Electromagnetics Research*, PIER 64, 69–80, 2006.
21. Manzanares-Martínez, J. and J. Gaspar-Armenta, "Direct integration of the constitutive of the relations for modeling dispersive metamaterials using the finite difference time-domain technique," *Journal of Electromagnetic Waves and Applications*, Vol. 21, No. 15, 2297–2310, 2007.
22. Schlager, K. L., "Relative accuracy of several finite-difference time domain methods in two and three dimensions," *IEEE Trans. on Antennas and Propagation*, Vol. 41 No. 12, 1732–1737, Dec. 1993.
23. Gao, S., L.-W. Li, and A. Sambell, "FDTD analysis of a dual-frequency microstrip patch antenna," *Progress In Electromagnetics Research*, PIER 54, 155–178, 2005.
24. Faghihi, F. and H. Heydari, "A combination of time domain finite element-boundary integral and with time domain physical optics for calculation of electromagnetic scattering of 3-D structures," *Progress In Electromagnetics Research*, PIER 79, 463–474, 2008.
25. Hoefer, W. J. R., "The TLM-method: Theory and applications," *IEEE Trans. Microwave Theory and Tech.*, Vol. 33, No. 10, 882–893, Oct. 1985.
26. Wienner, M., *Electromagnetic analysis using Transmission Line Variables*, World Scientific, New Jersey, 2001.
27. Russer, P., "The transmission line matrix method," *Applied Computational Methods*, NATO ASI series, 243–269, Springer, London, 2000.

28. Christopoulos, C. and P. Russer, "Application of TLM to EM problems," *Applied Computational Electromagnetic*, NATO ASI Series, 324–350, Springer, New York, 2000.
29. Pregla, R. and L. Vietzorreck, "Combination of the source method with absorbing boundary conditions in the method of lines," *IEEE Micro. Guided Wave Lett.*, Vol. 5, 227–229, July 1995.
30. Dreher A., and T. Rother, "New aspects of the method of lines,," *IEEE Micro. Guided Wave Lett.*, Vol. 5, 408–410, Nov. 1995.
31. Helfert, S. F., "Applying oblique coordinates in the method of lines," *Progress In Electromagnetics Research*, PIER 61, 271–278, 2006.
32. Preglas, R., "MOL-BPM method of lines based beam propagation method," *Progress In Electromagnetics Research*, PIER 11, 51–102, 1995.
33. Ney, M. M., "Method of moments as applied to electromagnetics problems," *IEEE Trans. Microwave Theory Tech.*, Vol. 33, 972–980, Oct. 1985.
34. Collin, R. E., *Field Theory of Guided Waves*, 2nd edition, IEEE Press, New York, 1991.
35. Grayaa, K., N. Hamdi, T. Aguili, and A. Bouallegue, "Full-wave analysis of shielded planar circuits using different models of sources," *IEE Proc. - Micro. Antennas Prop.*, Vol. 150, 258–264, Aug. 2003.
36. Alsunaidi, M. A., S. M. Simtiaz, and S. A. Ghazaly, "Electromagnetic wave effects on microwave transistors using a full-wave time domain model," *IEEE Trans. MTT*, Vol. 44, No. 6, 799–808, June 1996.
37. Baudrand, H. and D. Bajon, "Equivalent circuit representation for integral formulation of electromagnetic problems," *International Journal of Numerical Modeling*, Vol. 15, 23–57, Jan. 2002.
38. Pujol, S., H. Baudrand, V. F. Hanna, and X. Dong, "A new approach of the source method for characterization of planar structures," *EuMC*, 1015–1020, 1991.
39. Bajon, D. and H. Baudrand, "Application of wave concept iterative Procedure (WCIP) to Planar circuits," *Microtec'2000*, 864–868, Hanover, Sept. 2000.
40. Krokhin, A. A., I. B. Snapiro, and V. A. Yampol'skij, "Non-linear voltampere characteristic of a thin metallic foil with non diffuse faces," *Fizika Metallov i Metallovedenie (FMMTAK)*, Vol. 63, No. 3, 421–428, 1987.
41. Froelich, J., "Unital multiplications on a Hilbert space," *Proc. of*

*the Mathematical Society*, Vol. 117, No. 3, March 1993.

42. Istratescu, I., "Unimodular numerical contractions in Hilbert space," *Proc. Japan Acad.*, Vol. 47, 824–826, May 1971.
43. Stojmenović, I., *Handbook of Wireless Networks and Mobile Computing*, John Wiley & Sons, Inc., New York, 2002.
44. Yarkoni, N. and N. Blaunstein, "Prediction of propagation characteristics in indoor radio communication environments," *Progress In Electromagnetics Research*, PIER 59, 151–174, 2006.
45. Chen, C. H., C. L. Liu, C. C. Chiu, and T. M. Hu, "Ultrawide band channel calculation by SBR/Image techniques for indoor communication," *Journal of Electromagnetic Waves and Applications*, Vol. 20, No. 1, 41–51, 2006.
46. Abdi, A., H. M. El-Sallabi, L. Vuokko, and S. G. Haggman, "Spatial smoothing effect on kronecker MIMO channel model in urban microcells," *Journal of Electromagnetic Waves and Applications*, Vol. 21, No. 5, 681–696, 2007.
47. Kuo, L.-C. and H.-R. Chuang, "A study of planar printed dipole antennas for wireless communication applications," *Journal of Electromagnetic Waves and Applications*, Vol. 21, No. 5, 637–652, 2007.
48. Mahmoudian, A. and K. Forooragi, "A novel planar leaky wave antenna for wireless applications," *Journal of Electromagnetic Waves and Applications*, Vol. 22, 313–324, 2008.
49. Qin, W., "A novel patch antenna with a T-shaped parasitic strip for 2.4/5.8 GHz wlan applications," *Journal of Electromagnetic Waves and Applications*, Vol. 21, No. 15, 2311–2320, 2007.
50. Ayari, M., T. Aguili, and H. Baudrand, "An extended version of the differential-integral approach based on the transverse wave formulation," *ITST'06*, 457–460, Chengdu, China, June 2006.
51. Ayari, M., T. Aguili, and H. Baudrand, "Nouvelle formulation de l'approche en ondes transverses & applications aux antennes en réseaux périodiques," *OHD'05*, 54–59, Hammamet, Tunisia, Sept. 2005.
52. Tsai, E. Y., A. M. Bacon, M. Tentzeris, and J. Papapolymerou, "Design and development of novel micro-machined patch antenna for wireless applications," *Proc. Asian-Pacific Microwave Symposium*, 821–824, Nov. 2002.
53. Ayari, M., T. Aguili, and H. Baudrand, "An electromagnetic simulation tool based on the original Transverse Wave Approach (TWA)," *WorldComp'07*, Las Vegas, Nevada, USA, MSV7410, June 2007.